

**Friction Welding of 6061 Aluminum Alloy with YSZ-Alumina
Composite for Improved Mechanical and Thermal Properties**

By

UDAY MOWAFAK BASHEER

**Thesis submitted in fulfillment of requirements
For the degree of
Doctor of Philosophy**

February 2013

ACKNOWLEDGEMENTS

Alhamdulillah, all praises to Allah for his blessings and the strength given me to complete this thesis. Special appreciation goes to my main supervisor Prof. Dr. Ahmad Fauzi b. Mohd Noor for his supervisions and constant support. His invaluable help with constructive comments and suggestions throughout the experimental and thesis work have contributed to the success of this research. I would like also to express my sincere acknowledgment to my co-supervisors, Assoc. Prof. Mr. Ahmad Badri b. Ismail and Assoc. Prof. Dr. Zuhailawati bt. Hussain for their valuable guidance and comments during my study.

I would like to acknowledge the financial, academic and technical support given by Universiti Sains Malaysia, particularly awarding a Postgraduate Research Fellowship and USM-RU-PGRS grant no. 8042035 that provided the necessary financial support for this research.

Unforgettably, I would like to express my appreciation to the Dean Prof. Dr. Hanafi b. Ismail, Deputy Deans, lecturers and all the staff of the School of Materials and Mineral Resources Engineering, USM. My acknowledgement also goes to all the technicians and office staffs of our school for giving me their fullest co-operation.

My gratitude to my father for their infinite patience and implicit faith in my capabilities is boundless and cannot be expressed in sufficient words. I feel that my mother who passed away recently is looking at this work from the Heaven. I would like to extend my deepest thanks to my family (wife, sisters and daughters) for personal support and for their great patience at all times.

UDAY MOWAFAK BASHEER

TABLE OF CONTENTS

	Pages
ACKNOWLEDGEMENTS	ii
TABLE OF CONTENTS	iii
LIST OF TABLES	x
LIST OF FIGURES	xii
LIST OF ABBREVIATIONS	xxv
LIST OF SYMBOLS	xxvii
LIST OF PUBLICATIONS	xxx
ABSTRAK	xxxiii
ABSTRACT	xxxv
CHAPTER 1- INTRODUCTION	
1.1 Background	1
1.2 Problem Statement	4
1.3 Objectives of the Research	7
1.4 Research Approach	8
CHAPTER 2 - LITERATURE REVIEW	
2.1 Friction Welding	11
2.1.1 Energy Input Methods in Friction Welding	12
2.1.1.1 Direct Drive Welding	13
2.1.1.2 Inertia Drive Welding	14

2.1.2 Types of Friction Welding	16
2.1.2.1 Rotary Friction Welding	16
2.1.2.2 Orbital Friction Welding	17
2.1.2.3 Linear Friction Welding	18
2.1.2.4 Radial Friction Welding	19
2.1.2.5 Friction Stir Welding	20
2.1.3 Types of Relative Motion in Friction Welding Process	21
2.1.4 Advantages and Limitations of Friction Welding Process	23
2.1.5 Mechanism of Friction Welding	24
2.1.5.1 Friction Stage	24
2.1.5.2 Forging Stage	24
2.1.6 Parameters of Improving Friction Welding Joint	25
2.1.6.1 Rotational Speed	25
2.1.6.2 Friction Time	27
2.1.6.3 Joint Geometry	29
2.1.6.4 Friction Pressure	30
2.2 Effect of Thermal Analysis of Friction Welding Process	32
2.3 Effect of Thermal Stresses and Thermal Expansion on the Friction Welding	33
2.4 Temperature Distribution during Friction Welding	37
2.5 Heat Generation in Friction Welding	39
2.6 Effect of Friction Welding Conditions on Base Materials Joining	43
2.6.1 Combined Effect of Pressure and Temperature on the Metal Alloy	45
2.7 6061 Al Alloy	46
2.7.1 Friction Welding of Similar Al Alloy	47

2.7.2 Friction Welding of Al Alloy with Another Metal Alloys	49
2.8 Al ₂ O ₃ and Al ₂ O ₃ – ZrO ₂ Composite	53
2.8.1 Forming of Ceramic Composite by Slip Casting Process	56
2.8.2 Friction Welding of Ceramic Materials Reinforced with Al Alloy	57
2.8.3 Friction Welding of Al Alloy with Ceramics	58
2.9 Summary	62

CHAPTER 3- MATERIALS AND METHODOLOGY

3.1 Introduction	63
3.2 Raw Materials	63
3.2.1 Ceramic Materials	63
3.2.2 6061 Al Alloy	64
3.3 Samples Preparation for Friction Welding	64
3.3.1 Al Alloy Specimens Preparation	64
3.3.2 Forming of Ceramic Samples by Slip Casting	65
3.4 Friction Welding Process	68
3.5 Research Methodology	73
3.5.1 Concentration of YSZ Added to Al ₂ O ₃	74
3.5.2 Friction Time	75
3.5.3 Rotational Speed	75
3.5.4 Joint Geometry	76
3.5.5 Applied Pressure	78
3.6 Materials Characterization	79
3.6.1 X-Ray Fluorescence (XRF) Analysis	79

3.6.2 X-Ray Diffraction (XRD) Analysis	80
3.6.3 Particle Size Analysis	81
3.6.4 Particle Analysis Using FESEM and EDX Techniques	81
3.7 Density and Porosity Measurements	82
3.8 Thermal Expansion Analysis	84
3.9 Thermal Conductivity	85
3.10 Differential Scanning Calorimetry, DSC Analysis	88
3.11 Mechanical Properties and Microstructure Analysis	89
3.11.1 Vickers Microhardness Tests	89
3.11.2 Four-Point Bending Strength	90
3.11.3 Optical Microscopy at the Interface Zone	91
3.11.4 FESEM and EDX Analysis	92
3.11.5 Fractography	93
3.12 Further Analysis on the Base Materials after Friction Welding	93
3.13 Thermal Properties Analysis during Friction Welding Process	94
3.13.1 Temperature Measurements	94
3.13.2 Frictional Heat Generation	94

CHAPTER 4 - RESULT AND DISCUSSION

4.1 Introduction	97
4.2 Raw Materials Characterization	97
4.2.1 X-Ray Fluorescence (XRF) Analysis	97
4.2.2 X-Ray Diffraction (XRD) Analysis	98
4.2.3 Particle Size Analysis	102

4.2.4 FESEM and EDX Analysis	103
4.3 Specimens Preparation	107
4.3.1 Al Alloy Specimens Preparation	107
4.3.2 Forming of Ceramic Specimens	107
4.3.2.1 Al ₂ O ₃ Specimens	107
4.3.2.2 Al ₂ O ₃ / YSZ Composite Specimens	109
4.4 Thermal Expansion	113
4.5 Thermal Conductivity, Thermal Diffusivity and Heat Capacity	116
4.5.1 Influence of the Porosity on the Thermal Conductivity	121
4.6 Differential Scanning Calorimetry (DSC) Analysis	123
4.7 Influence of Rotational Speeds on the Joint Characteristics	124
4.7.1 Microstructure of Friction Welding between Al ₂ O ₃ and 6061 Al Alloy	125
4.7.1.1 Optical Microscopy Microstructure at the Interface Zone	125
4.7.1.2 Scanning Electron Microscopy Microstructure at the Interface Zone	127
4.7.1.3 EDX Analysis of Al ₂ O ₃ – Al alloy	131
4.7.2 Deformation Zone and Grain Size of Al ₂ O ₃ –6061 Al Alloy	137
4.7.3 Mechanical Properties of Friction Welding Al ₂ O ₃ –Al Alloy	138
4.7.3.1 Vickers Microhardness Tests	138
4.7.3.2 Four-Point Bending Strength	139
4.7.3.3 Fracture Surface Analysis of the Al ₂ O ₃ and Al Alloy Joints	141
4.7.4 Microstructure of Friction Welding between Al ₂ O ₃ - YSZ and 6061 Al Alloy	144
4.7.4.1 Optical Microscopy Microstructure at the Interface Zone	145
4.7.4.2 Scanning Electron Microscopy Microstructure at the Interface Zone	150

4.7.4.3 EDX Line Analysis	158
4.7.4.4 Deformation Zone and Grain Size of Al ₂ O ₃ -YSZ to 6061 Al Alloy	163
4.7.4.5 Vickers Microhardness Test	165
4.7.4.6 Four-Point Bending Strength	168
4.7.4.7 Fracture Surface Analysis of Al ₂ O ₃ -YSZ and Al Alloy Joints	169
4.8 Influence of Friction Time on the Friction-Welding Joint	175
4.8.1 Microstructure Observation	175
4.8.2 Four-Point Bending Strength	177
4.9 Influence of Joint Geometries	180
4.9.1 Effect of the Joint Geometry on the Microstructure of the Weld	182
4.9.2 Effect of the Joint Geometry on the Mechanical Properties of the Weld	189
4.9.2.1 Vickers Microhardness Tests	189
4.9.2.2 Four-Point Bending Strength	191
4.9.2.3 Fractography	195
4.10 Further Analysis on the Base Materials after Friction Welding	201
4.10.1 Effect of Fracture Mechanics on the Ceramic	201
4.10.2 Deformation Behavior on the Al Alloy after Friction Welding	206
4.10.2.1 Al Alloy Characterization near the Weld Interface	207
4.10.2.2 Supporting Microstructural Observation and XRD near the Interface	216
4.10.2.3 Al Alloy Characterization after the Weld Interface in Friction Welding	219
4.11 Thermal Properties Analysis during Friction Welding Process	230
4.11.1 Temperature Measurements	230

4.11.2.1 Variation of Friction Temperature with Respect to Rotational Speeds	230
4.11.2.2 Variation of Friction Temperature with Respect to Friction Time	231
4.11.2.3 Variation of Friction Temperature with Respect to Joint Geometries	233
4.11.2 Frictional Heat Generation	234
4.11.2.1 Effect of Rotational Speeds on the Frictional Heat Generation	235
4.11.2.2 Effect of Joint Geometry on the Frictional Heat Generation	236
CHAPTER 5 - CONCLUSION AND RECOMMENDATION	
5.1 Conclusion	239
5.2 Recommendation for Future Research	241
REFERENCES	242
APPENDICES	
APPENDIX A	XRD REFERENCES FILES
APPENDIX B	PARTICLE SIZE DISTRIBUTION
APPENDIX C	HOT DISK TECHNIQUE RESULTS
APPENDIX D	RELEVANT PARAMETERS OF BULK SAMPLES
APPENDIX E	PUBLISHED PAPERS

LIST OF TABLES

	Pages
Table 2.1: Properties of 6061 Al alloy	47
Table 2.2: Friction weldability of Al and Al alloys to other metals	50
Table 2.3: Properties of Al ₂ O ₃ and YSZ	55
Table 3.1: The dimensions of the four ceramic shapes used for friction welding	77
Table 3.2: The friction welding process parameters studied	78
Table 3.3: The variables used for heat generation calculation with different rotational speeds	96
Table 3.4: The variables used for heat generation calculation with joint geometries	96
Table 4.1: Chemical composition of the 6061 Al Alloy by XRF technique	98
Table 4.2: Chemical composition of the Al ₂ O ₃ by XRF technique	98
Table 4.3: Chemical composition of the YSZ by XRF technique	98
Table 4.4: Relevant parameters of Al ₂ O ₃ powder from XRD	99
Table 4.5: Relevant parameters of YSZ from XRD	100
Table 4.6: Relevant parameters of 6061 Al alloy from XRD	101
Table 4.7: The rheological properties of the Al ₂ O ₃ suspension	107
Table 4.8: The bulk density, porosity and shrinkage results of the Al ₂ O ₃ using Archimedes method	108
Table 4.9: The rheological properties of the Al ₂ O ₃ -YSZ suspension at 25°C	110
Table 4.10: The density, porosity and shrinkage results of the Al ₂ O ₃ -YSZ composite	111
Table 4.11: Bulk density and theoretical density of the ceramic compositions investigated	122

Table 4.12:	The experimental parameters when examining the influence of rotational speeds	125
Table 4.13:	The parameters used for the experiments	182
Table 4.14:	Results of friction welding process parameters on the 6061 Al alloy	209
Table 4.15:	XRD results of 6061Al alloys with Al ₂ O ₃ -25wt% YSZ composite joint at different rotational speed near the interface	216
Table 4.16:	XRD results of 6061Al alloys with Al ₂ O ₃ -25wt% YSZ composite joint at different rotational speed in the 0.5 mm distance	225
Table 4.17:	XRD results of 6061Al alloys with Al ₂ O ₃ -25wt% YSZ composite joint at different rotational speed in the 1 mm distance	226
Table 4.18:	XRD results of 6061Al alloys with Al ₂ O ₃ -25wt% YSZ composite joint at different rotational speed in the 3 mm distance	227
Table 4.19:	XRD results of 6061Al alloys with Al ₂ O ₃ -25wt% YSZ composite joint at different rotational speed in the 5 mm distance	228

LIST OF FIGURES

Figure 1.1:	Flowchart of research stage one, ceramic composite preparation	9
Figure 1.2:	Flowchart of research stage two, 6061 Al alloy preparation	10
Figure 1.3:	Flowchart of research stage three, friction welding process	10
Figure 2.1:	Basic steps in friction welding	12
Figure 2.2:	Basic arrangement of a direct drive-welding machine	13
Figure 2.3:	Direct drive friction welding parameter characteristics	14
Figure 2.4:	Basic arrangement of an inertia-welding machine	15
Figure 2.5:	Inertia friction welding parameter characteristics	15
Figure 2.6:	Rotary friction welding process	17
Figure 2.7:	Schematic diagram of the orbital friction welding process	18
Figure 2.8:	Schematic diagram of the linear friction welding process	19
Figure 2.9:	Schematic diagram of the radial friction welding process	20
Figure 2.10:	Friction stir welding process	21
Figure 2.11:	Typical Arrangements of Friction Welding	22

Figure 2.12:	FESEM micrograph taken from the welding interface of the specimen with 1500 rpm	27
Figure 2.13:	Tensile tested FESEM fracture surface (a)10 μ m and (b)50 μ m	29
Figure 2.14:	The size of workpieces for: (A)Joint system 1 and (B) Joint system 2	31
Figure 2.15:	Comparison of CTE of metals and ceramics	35
Figure 2.16:	Effect of size and shape of bond face on residual stress of Si ₃ N ₄ / invar alloy joints. The residual stress was vertical to the interface on the Si ₃ N ₄ surface	36
Figure 2.17:	Idealized heat flow model for friction welding of rods; (a) Sketch of model and (b) Subdivision time into series of infinitesimal elements d _t	38
Figure 2.18:	Schematic arrangement of friction welding of a solid rod	41
Figure 2.19:	Schematic diagram showing the three main reaction zones within a friction welded component (Z _{pi} \ fully plasticized region, Z _{pd} \ partly deformed region, Z _{ud} \ undeformed region	43
Figure 2.20:	Materials behavior under stress	45
Figure 2.21:	(a) Microstructure of friction welding of Al alloy (AA7075-T6), SS= stationary side, RS= rotating side and (b) Mid radius	49
Figure 2.22:	FESEM morphology of fracture surface on side of nodular cast iron	52
Figure 2.23:	Binary equilibrium phase diagram of ZrO ₂ -Al ₂ O ₃ system	56
Figure 2.24:	The micrograph of weld zone of (a) Al ₂ O ₃ 5 vol. % (60 μ m average particle sizes) reinforced with 6061 Al alloy and SAE 1020 steel and (b) Al ₂ O ₃ 15 vol. % (60 μ m average particle size) reinforced with 6061 Al alloy and SAE 1020 steel	58
Figure 2.25:	Schematic diagrams of friction welding	60
Figure 2.26:	Shapes and dimensions of specimens used for friction welding (a) bar and (b) pipe	61

Figure 2.27:	Mechanical interlocking between Al ₂ O ₃ -Al, (a) friction times of 18 sec, (b) friction times of 16 sec and (c) friction times of 14 sec	62
Figure 3.1:	The 6061 Al alloy rods samples were (a) machined down to the diameter required, and (b) facing off using a lathe machine	65
Figure 3.2:	Schematic of slip casting process	67
Figure 3.3:	Schematic diagram of pre-sintering profile of ceramic sample	67
Figure 3.4:	Schematic diagram of final sintering profile of ceramic sample	68
Figure 3.5:	A modified lathe machine with hydraulic press used as friction welding machine	69
Figure 3.6:	A set up of a friction-welding machine	70
Figure 3.7:	Illustration of the rotary and stationary jaw used in friction welding machine	70
Figure 3.8:	The supporter for ceramic composite samples made from Al	71
Figure 3.9:	Photo shows the second piston	72
Figure 3.10:	The size of specimens for (a) Flat ceramic shape, (b) Taper pin angle 60° ceramic shape, (c) Taper pin angle 30° ceramic shape and (d) Pin ceramic shape to constant flat metal shape	77
Figure 3.11:	Photos show a hot disk (TPS element / sensor)	86
Figure 3.12:	Schematic shows the experiment arrangement the sensor clamped between the sample halves measuring the thermal conductivity	87
Figure 3.13:	The experiment is performed by recording the voltage / resistance variations over the TPS element (a) Hot Disk TPS1500 and (b) Furnace chamber	88
Figure 3.14:	(a) Picture of axial torsion test system machine, and (b) Test layout for the 4- point bending test	91

Figure 3.15:	Schematic diagram of bending test between Al ₂ O ₃ -YSZ composite and 6061 Al alloy joint	91
Figure 3.16:	6061 Al alloy rotating against Al ₂ O ₃ -YSZ composite, Assume that the friction force (F_f), linear velocity (V), contact area (A_c) and heat flux (q) from ceramic composite to 6061 Al alloy	95
Figure 4.1:	The XRD spectrum of Al ₂ O ₃ powder	99
Figure 4.2:	The XRD spectrum of YSZ powder	100
Figure 4.3:	The XRD spectrum of 6061 Al alloy	101
Figure 4.4:	Result of the particle size analysis of Al ₂ O ₃ powder	102
Figure 4.5:	Result of particle size of YSZ	103
Figure 4.6:	(a) Micrograph of Al ₂ O ₃ particle and (b) EDX results of the Al ₂ O ₃ powder	104
Figure 4.7:	(a) Micrograph of YSZ particle and (b) EDX results of the YSZ powder	105
Figure 4.8:	(a) Micrograph of 6061 Al alloy grains and (b) EDX results of the 6061 Al alloy	106
Figure 4.9:	The dimensions of the 6061 Al alloy specimens used for this study	107
Figure 4.10:	Photos of Al ₂ O ₃ ceramic specimen, (a) and (b) Pre-sintering of alumina at 1200°C, while (c) and (d) Final sintering at 1600 °C	108
Figure 4.11:	Microstructure of Al ₂ O ₃ at 1600°C observed under FESEM (a) 500X and (b) 1000X	109
Figure 4.12:	Photos of Al ₂ O ₃ -YSZ ceramic composite sample, (a) and (b) Pre-sintering of composite at 1200 °C, while (c) and (d) Final sintering at 1600 °C	111

Figure 4.13:	The microstructure of the Al ₂ O ₃ -YSZ composite at 1600°C observed under FESEM: (a) YSZ grain in the surface at 1000X, (b) 3000X	112
Figure 4.14:	(a) Microstructure of Al ₂ O ₃ -YSZ composite at 1600°C observed under FESEM and (b) EDX results of the Al ₂ O ₃ -YSZ composite	114
Figure 4.15:	Thermal expansion of the Al ₂ O ₃ -YSZ composites and 6061 Alloy	115
Figure 4.16:	Delta L/L° Of the Al ₂ O ₃ -YSZ composites and 6061Al Alloy	115
Figure 4.17:	Thermal Conductivity of pure Al ₂ O ₃ and Al ₂ O ₃ 25 and 50 wt% YSZ composite with increase temperature	118
Figure 4.18:	Thermal Diffusivity of pure Al ₂ O ₃ and Al ₂ O ₃ -25 and 50 wt% YSZ composite with increase temperature	120
Figure 4.19:	Specific heat of Al ₂ O ₃ and Al ₂ O ₃ -0, 25 and 50 wt% YSZ composite with increase temperature	121
Figure 4.20:	Influence of the porosity on the thermal conductivity of Al ₂ O ₃ and Al ₂ O ₃ -25, 50 wt% YSZ with different temperatures	123
Figure 4.21:	DSC heat flow curves for the 6061 Al alloy, pure Al ₂ O ₃ and Al ₂ O ₃ -25, 50 wt % YSZ with increasing temperature to 300°C	124
Figure 4.22:	Optical images of interface properties of specimens welded at (a, b)1250rpm, (c, d)1800 rpm, (e, f) 2500 rpm magnification 100X ,200X	127
Figure 4.23:	Interface of specimen welded observed under FESEM at 1250 rpm (a) 1000X and (b) 5000X	129
Figure 4.24:	Interface of specimen welded observed under FESEM at 1800 rpm (a) 1000X and (b) 5000X	129
Figure 4.25:	Interface of specimen welded observed under FESEM at 1800 rpm after etching in 1% NaOH, time=15min	130
Figure 4.26:	Interface of specimen welded observed under FESEM at 2500 rpm (a) 1000X and (b) 3000X	131
Figure 4.27:	Shapes of Burrs in the joining between Al ₂ O ₃ -6061 Al Alloy (a) 1250 rpm, (b) 2500 rpm	131

Figure 4.28:	Micrograph joint of Al ₂ O ₃ to 6061 Al alloy at 1250 rpm with EDX analysis at (1) point A (2) point B (3) point C (4) point D and (5) at point E	132
Figure 4.29:	FESEM microstructure of Al ₂ O ₃ -6061 Al alloy interface and EDX line scans result at 1250 rpm	133
Figure 4.30:	FESEM microstructure of Al ₂ O ₃ -6061 Al alloy interface and EDX line scans result at 1800 rpm	135
Figure 4.31:	FESEM microstructure of Al ₂ O ₃ -6061 Al alloy interface and EDX line scans result at 2500rpm	136
Figure 4.32:	Grain structure distribution exhibited within the three different zones (A, B and C) at the friction weld interface between Al ₂ O ₃ and 6061 Al alloy at rotational speed 1800 rpm	138
Figure 4.33:	Microhardness traverse of pure Al ₂ O ₃ -6061 Al alloy friction welded joints: (a) Al ₂ O ₃ side and (b) 6061 Al side	139
Figure 4.34:	Four point bending strength of Al ₂ O ₃ -6061 Al alloy friction welded joints	140
Figure 4.35:	FESEM fractography of pure Al ₂ O ₃ -6061 Al alloy joint at rotational speed 1250 rpm (a) 500X and (b) 1000X	142
Figure 4.36:	FESEM fractography of pure Al ₂ O ₃ / 6061 Al alloy joint at rotational speed 1800 rpm (a) 500X, (b) 1000X, showing brittle fracture	142
Figure 4.37:	FESEM fractography of pure Al ₂ O ₃ / 6061 Al alloy joint at rotational speed 2500rpm (a) An overview of the fracture surface which is composed of zone A with brittle fracture and zone B which exhibits characteristics of ductile fractures (500×). (b) A high magnification view of the ductile fracture area zone A (1000×)	143
Figure 4.38:	FESEM micrographs showing fracture surface feature of pure alumina sample taken from joint with 6061 Al alloy after four point bending test	144
Figure 4.39:	Cross-section of Al ₂ O ₃ -25-wt % YSZ / 6061 Al Alloy with speed of 630rpm (a) 100X and (b) 200X	145
Figure 4.40:	Cross-section of Al ₂ O ₃ -25 wt % YSZ / 6061 Al Alloy with speed of 900 rpm (a) 100X and (b) 200X	146

Figure 4.41:	Cross-section of Al ₂ O ₃ -50 wt % YSZ / 6061 Al Alloy with speed of 900 rpm (a) 100X and (b) 200X	146
Figure 4.42:	Cross-section of Al ₂ O ₃ -25 wt % YSZ / 6061 Al Alloy with speed of 1250 rpm (a) 100X and (b) 200X	147
Figure 4.43:	Cross-section of Al ₂ O ₃ -50 wt % YSZ / 6061 Al Alloy with speed of 1250rpm 100X, (a) current interface. (b)Some porous inside ceramic surface	147
Figure 4.44:	Cross-section of Al ₂ O ₃ -25 wt % YSZ / 6061 Al Alloy with speed of 1800rpm (a) 100X and (b) 200X	148
Figure 4.45:	Cross-section of Al ₂ O ₃ -50 wt % YSZ / 6061 Al Alloy with speed of 1800 rpm (a) 100X and (b) 200X	148
Figure 4.46:	Cross-section of Al ₂ O ₃ -25 wt % YSZ / 6061 Al Alloy with speed of 2500 rpm (a) 100X and (b) 200X	149
Figure 4.47:	Interface of Al ₂ O ₃ -25 wt % YSZ / 6061 Al alloy welded observed under FESEM at 630 rpm (a) 1000X and (b) 3000X	152
Figure 4.48:	Interface of Al ₂ O ₃ -25 wt % YSZ / 6061 Al alloy welded observed under FESEM at 900 rpm (a) 1000X and (b) 3000X	152
Figure 4.49:	Interface of Al ₂ O ₃ -50 wt% YSZ / 6061 Al alloy welded observed under FESEM at 900 rpm (a) 1000X and (b) 3000X	153
Figure 4.50:	Interface of Al ₂ O ₃ -25 wt% YSZ / 6061 Al alloy welded observed under FESEM at 1250rpm (a) 1000X and (b) 3000X	155
Figure 4.51:	Interface of Al ₂ O ₃ -50 wt. % YSZ / 6061 Al alloy welded observed under FESEM at 1250 rpm (a) 100X and (b) 500X	155
Figure 4.52:	Interface of Al ₂ O ₃ -25wt% YSZ/6061 Al alloy welded observed under FESEM at 1800 rpm (a) 500X and (b) Unbonded area and (C) Bonded area (3000X)	156
Figure 4.53:	Interface of Al ₂ O ₃ -50 wt. % YSZ / 6061 Al alloy welded observed under FESEM at 1800 rpm (a) 300X and (b) 1000X	157
Figure 4.54:	FESEM microstructure of central interface and EDX line scans result at 630 rpm	159
Figure 4.55:	FESEM microstructure of central interface and EDX line scans result at 900 rpm	160

Figure 4.56:	FESEM microstructure of central interface and EDX line scans result at 1250 rpm	161
Figure 4.57:	FESEM microstructure of central interface and EDX line scans result at 1800 rpm	162
Figure 4.58:	Microstructural classification of friction-welded YSZ-Al ₂ O ₃ with 6061 Al Alloy joints showing three regions (a) Unaffected zone (UZ), (b) deformed zone (DZ), (c) nearest interface transformed and recrystallized fully deformed zone (FPDZ)with magnification 3000X	165
Figure 4.59:	Microhardness traverse of Al ₂ O ₃ – 25 wt% YSZ composite / 6061 Al alloy friction welded joints: (a) ceramic side and (b) metal side	167
Figure 4.60:	Microhardness traverse of Al ₂ O ₃ – 50 wt %YSZ composite / 6061 Al alloy friction welded joints (a) ceramic side and (b) metal side	167
Figure 4.61:	Four point bending strength of Al ₂ O ₃ -YSZ composite / 6061 Al alloy friction welded joints	169
Figure 4.62:	Fracture surface of 6061 Al alloy sample joint with Al ₂ O ₃ -25 wt %YSZ composite after four point bending test at rotational speeds 630 rpm	171
Figure 4.63:	Fracture surface of 6061 Al alloy sample joint with Al ₂ O ₃ -25 wt %YSZ composite after four point bending test at rotational speeds 900 rpm	171
Figure 4.64:	Fracture surface of Al ₂ O ₃ -25 wt %YSZ composite with 6061 Al alloy joint at rotational speed 1250 rpm (a) 500X and (b) 1000X	172
Figure 4.65:	Fracture surface of Al ₂ O ₃ -25 wt %YSZ composite with 6061 Al alloy joint at rotational speed 1800 rpm (a) 1000X and (b) 3000X	172
Figure 4.66:	Fracture surface of Al ₂ O ₃ -50 wt % YSZ composite with 6061 Al alloy joint at rotational speed 900 rpm (a) 500X and (b) 1000X	173
Figure 4.67:	FESEM micrographs showing fracture surface feature of Al ₂ O ₃ -25wt % YSZ sample taken from joint with 6061 Al alloy after four point bending test	174

Figure 4.68:	FESEM micrographs showing fracture surface feature of Al_2O_3 -50wt % YSZ sample taken from joint with 6061 Al alloy after four point bending test	174
Figure 4.69:	Interface of Al_2O_3 -6061 Al alloy welded observed under FESEM at 1250-rpm speed, 60 sec time	176
Figure 4.70:	Interface of Al_2O_3 -25 wt. % YSZ / 6061 Al alloy welded observed under FESEM at 1250rpm speed, 60 sec time	177
Figure 4.71:	Interface of (a) pure Al_2O_3 (b) Al_2O_3 - 25 wt. % YSZ / 6061 Al alloy welded observed under FESEM at 1250rpm speed, 30 sec time	177
Figure 4.72:	Four point bending strength of pure Al_2O_3 -6061 Al alloy friction welded joints with different friction time	179
Figure 4.73:	Four point bending strength of Al_2O_3 -25wt% / 6061 Al alloy friction welded joints with different friction time	180
Figure 4.74:	Four point bending strength of Al_2O_3 -50wt% / 6061 Al alloy friction welded joints with different friction time	180
Figure 4.75:	Micro cross-section views of friction zone welded by, (a) flat ceramic face to flat metal face, (b) taper pin angle 60° ceramic face to flat metal face, (c) taper pin angle 30° ceramic face to flat metal face, (d) pin ceramic face to flat metal face	183
Figure 4.76:	Microstructures of friction welded between ceramic and 6061 Al alloy flat shape (Type 1), (A) Deformed zone, (B) Undeformed zone	184
Figure 4.77:	Microstructures of friction welded between Al_2O_3 and 6061 Al alloy with Taper pin angle 30° at (a) 50X and (b) 100X	184
Figure 4.78:	Microstructures of friction welded between Al_2O_3 and 6061 Al alloy with pin shape (Type 4), (A) Fully deformed zone, (B) Deformed zone and (C) Undeformed zone	185
Figure 4.79:	Optical images of interface properties of the taper pin 60° specimen in the weld deformation zone.(A) Fully deformed zone, (B) Deformed zone and (C)Undeformed zone	187
Figure 4.80:	Grain structure distribution exhibited within the three different zones at the friction weld interface between Al_2O_3 and 6061 Al alloy, (a) recrystallized fully deformed zone (FPDZ), (b) deformed zone (DZ) and (c) unaffected zone (UZ)	188

Figure 4.81:	Microhardness traverse of Al ₂ O ₃ -6061 Al alloy friction welded joints with different ceramic shapes (a) Ceramic side and (b) Metal side	190
Figure 4.82:	Microhardness traverse of Al ₂ O ₃ -25 wt% YSZ composite - 6061 Al alloy friction welded joints with different ceramic shapes (a) Ceramic side and (b) Metal side	190
Figure 4.83:	Four-point bending strength of pure Al ₂ O ₃ -6061 Al alloy friction welded joints with different rotational speeds and ceramic face shapes	192
Figure 4.84:	Four-point bending strength of Al ₂ O ₃ -6061 Al alloy friction welded joints with different ceramic shapes at 1250 rpm	192
Figure 4.85:	Four-point bending strength of Al ₂ O ₃ -25 wt % YSZ / 6061 Al alloy friction welded joints with different rotational speeds and ceramic face shapes	194
Figure 4.86:	Four-point bending strength of Al ₂ O ₃ -25 wt % YSZ / 6061 Al alloy friction welded joints with different ceramic shapes	194
Figure 4.87:	FESEM fractography of Al ₂ O ₃ flat shape with 6061 Al alloy joint at rotational speed 1250rpm :(a) 500X and (b) 3000X.	196
Figure 4.88:	FESEM fractography of Al ₂ O ₃ taper pin 60 shape with 6061 Al alloy joint at rotational speed 1250rpm:(a) 500X and (b) 1000X	197
Figure 4.89:	FESEM micrographs showing fracture surface feature of Al ₂ O ₃ samples taken from joint with 6061 Al alloy after four point bending test. (a) 500X and (b) 1000X	197
Figure 4.90:	FESEM fractography of Al ₂ O ₃ taper pin 30° shape with 6061 Al alloy joint at rotational speed 1250rpm:(a) 500X and (b) 1000X	198
Figure 4.91:	FESEM fractography of Al ₂ O ₃ pin shape with 6061Al alloy joint at rotational speed 1250rpm :(a)200X and (b)1000X	199
Figure 4.92:	FESEM fractography of Al ₂ O ₃ -25 wt% YSZ composite flat shape with 6061 Al alloy joint at low rotational speed 630 rpm (a) 500X and (b) 1000X	200

Figure 4.93:	FESEM fractography of Al ₂ O ₃ -25 wt% YSZ composite taper pin 30° shape with 6061 Al alloy joint at rotational speed 1250 rpm :(a) 500X and (b) 1000X	200
Figure 4.94:	FESEM fractography of Al ₂ O ₃ -25 wt% YSZ composite taper pin 60° shape with 6061 Al alloy joint at rotational speed 1250 rpm:(a) 500X and (b) 1000X	201
Figure 4.95:	Appearances of friction welded interfaces after welding pure Al ₂ O ₃ with 6061 Al alloy at different rotational speeds	202
Figure 4.96:	Fracture appearances of friction welded interfaces after welding Al ₂ O ₃ - 25, 50 wt % YSZ composite with 6061 Al alloy at different rotational speeds	203
Figure 4.97:	The crack tips tend to form at a zigzag or curvature of micro - dimensions in very brittle ceramics	203
Figure 4.98:	FESEM micrograph showing fracture surface feature of Al ₂ O ₃ -25 wt % YSZ composite taken from joint with 6061 Al alloy after bending test	204
Figure 4.99:	XRD pattern of (a) bulk pure Al ₂ O ₃ , (b) Al ₂ O ₃ - 25 wt % YSZ composite and (c) Al ₂ O ₃ -50 wt % YSZ composite.	205
Figure 4.100:	Microstructure of base 6061 Al Alloy without deformation (a) 500X and (b) 1000X	207
Figure 4.101:	The deformation in the 6061 Al alloy after joining with ceramic at different rotational speeds	208
Figure 4.102:	The dimensions of metal bars before and after joining with ceramic bars with different rotational speeds	210
Figure 4.103:	Fracture surfaces of the 6061 Al alloy interface after joining with ceramic composite at rotational speed 630 rpm	211
Figure 4.104:	Fracture surfaces of the 6061 Al alloy interface after joining with ceramic composite at rotational speed 900 rpm	212
Figure 4.105:	Fracture surfaces of the 6061 Al alloy interface after joining with ceramic composite at rotational speed 1250 rpm	213
Figure 4.106:	Fracture surfaces of the 6061 Al alloy interface after joining with ceramic composite at rotational speed 1800 rpm	214

Figure 4.107:	Fracture surfaces of the 6061 Al alloy interface after joining with Al ₂ O ₃ -25 wt % YSZ composite at rotational speed 2500 rpm	215
Figure 4.108:	XRD profiles for 6061 Al alloy deformation near interface surface with Al ₂ O ₃ -25 wt % YSZ joint at different rotational speeds	217
Figure 4.109:	The recrystallized microstructure is formed as a result of the mechanical action of the friction phenomena that generates a continuous dynamic recrystallization process	218
Figure 4.110:	The cross sectional view representation of friction-welded ceramic and 6061 Al alloy showing the locations cutting surfaces with different positions	220
Figure 4.111:	Microstructure of the 6061 Al Alloy with deformation at the position 0.5 mm at high rotational speed (a) 630 rpm (b) 1250 rpm (c) 1800 rpm and (d) 2500 rpm	221
Figure 4.112:	Microstructure of the 6061 Al Alloy with deformation at the position 1mm for rotational speed (a) 630 rpm, (b) 1250 rpm, (c) 1800 rpm, (d) 2500 rpm	222
Figure 4.113:	Microstructure of the 6061 Al Alloy with (a) deformation at the position 3mm compared with (b) base metal alloy	223
Figure 4.114:	Microstructure of the 6061 Al Alloy with deformation at the position 3mm for rotational speed (a) 630 rpm, (b) 1250 rpm, (c) 1800 rpm, (d) 2500 rpm	223
Figure 4.115:	Microstructure of the 6061 Al Alloy with deformation at the position 5 mm for rotational speed 1250 rpm	224
Figure 4.116:	XRD profiles for 6061 Al alloy deformation (0.5 mm distance) with ceramic composite joint at different rotational speeds	225
Figure 4.117:	XRD profiles for 6061 Al alloy deformation (1mm distance) with ceramic joint at different rotational speeds	226
Figure 4.118:	XRD profiles for 6061 Al alloy deformation (3mm distance) with ceramic joint at different rotational speeds	227
Figure 4.119:	XRD profiles for 6061 Al alloy deformation (5mm distance) with ceramic joint at different rotational speeds	228

Figure 4.120:	Effect of the crystallize size with increasing the rotational speeds	229
Figure 4.121:	Effect of rotational speed on the friction temperature of the joining between pure Al ₂ O ₃ , Al ₂ O ₃ 25, 50 wt % YSZ and 6061 Al alloy	231
Figure 4.122:	Effect of friction time with the friction temperature of the joining between pure Al ₂ O ₃ and 6061 Al alloy	232
Figure 4.123:	Effect of friction time with the friction temperature of the joining between Al ₂ O ₃ -25% YSZ and 6061 Al alloy	232
Figure 4.124:	Effect of friction time with the friction temperature of the joining between Al ₂ O ₃ -50% YSZ and 6061 Al alloy	233
Figure 4.125:	Effect of joint geometry on the friction-welded temperature of the joining between pure Al ₂ O ₃ , Al ₂ O ₃ -25 wt % YSZ and 6061 Al alloy joined at 1250 rpm	234
Figure 4.126:	Effect of rotational speed on the frictional heat generation of the joining between pure Al ₂ O ₃ , Al ₂ O ₃ – YSZ composite and 6061 Al alloy	236
Figure 4.127:	Effect of rotational speed on the frictional heat flux of the joining between pure Al ₂ O ₃ , Al ₂ O ₃ - YSZ and 6061 Al alloy	236
Figure 4.128:	Effect of joint geometry on the frictional heat generation with different rotational speeds	237
Figure 4.129:	Effect of joint geometry on the frictional heat flux with different rotational speeds	238

LIST OF ABBREVIATIONS

Abbreviation	Description
6061 Al	Precipitation Hardening Aluminum Alloy
Al ₂ O ₃	Aluminum Oxide
BSE	Back-Scattered Electrons
CTE	Coefficient of Thermal Expansion
DRX	Dynamically Recrystallized Zone
DSC	Differential Scanning Calorimetry
DZ	Deformed Zone
EDX	Energy-Dispersive X-ray Spectroscopy
EMPA	Electron Microprobe Analysis
FESEM	Field Emission Scanning Electron Microscope
FPDZ	Full Plastic Deformed Zone
FSW	Friction Stir Welding
FW	Friction Welding
HAZ	Heat Affected Zone
LFW	Linear Friction Welding
MMC	Metal Matrix Composite
NaOH	Sodium Hydroxide
OM	Optical Microscope
pH	Concentration of hydrogen's ions
PM	Powder Metallurgy
POP	Plaster Of Paris

PVA	Poly Vinyl Alcohol
RPM	Revolutions Per Minute
SE	Secondary Electrons
T	Tetragonal Phase
TMAZ	Thermomechanically Affected Zone
TPS	Thermal Constants Analyzer
UZ	Unaffected Zone
Wt.	Weight
XRD	X-ray Diffraction
XRF	X-ray Fluorescence
YSZ	Yttria Stabilized Zirconia
Z_{pd}	Partly Deformed Region
Z_{pl}	Fully Plasticized Region
ZrO_2	Zirconium Oxide
Z_{ud}	Undeformed Region

LIST OF SYMBOLS

Symbol	Description
Δl	Change in length
ΔL	Change in length of the test piece (mm)
$\Delta T(t)$	Time- dependent temperature increase of the TPS element
μ	Friction coefficient
a_1	Radius of the sensor
A_{11}	Cross section area (mm ²)
a_2	Thermal diffusivity, mm ² s ⁻¹
a_3	Distance between the supporting and the loading pins
A	Area of the sample
A_1	Surface area of the small piston
A_2	Surface area of the second piston
A_c	Contact area
B	Burn-off length
d	Arithmetic mean of two diagonal lengths (mm)
D	Section diameter of round specimen
$D(\tau)$	Theoretical expression of the time dependent temperature
d_t	Subdivision time into series of infinitesimal elements
F	Force applied
F_f	Friction force
F_g	Forge pressure
F_M	Maximum bending force

H_v	Vickers hardness
k	Thermal conductivity (W / (m· °K))
L	Load
L_0	Original test piece length
M	Interfacial torque
P	Friction pressure (N. mm ⁻²)
$P(r)$	Pressure distribution across the interface
P_a	Apparent porosity
P_o	Total output power
P_T	Applied load (Newton)
q	Heat flows through a material (W)
q	Heat flux
Q	Thermal energy generation
q_o	Net heat power (Watt)
Q_s	Heat generated from the shoulder/plate interface
r	Radius of samples
R°	Surface radius
R_1	Radius of the small piston
R_2	Radius of the second piston
R_o	Resistance of TPS element
t	Time, second
t'_h	Duration of heating period, second
T_1	Reference temperature (°K)

T_2	Test temperature (°K)
T_h	Temperature at the end of the heating period, °C
$T_{M.P.absolute}$	Melting point absolute temperature
T_o	Ambient temperature, °C
T_{sp}	Apparent specific gravity
u_{max}	Maximum surface velocity at the outer edge (m s ⁻¹)
V	Exterior volume (cm ³)
V	Linear velocity
V_{IP}	Impervious portions (cm ³)
V_{OP}	Volumes of open pores (cm ³)
W_d	Dry weight of sintered sample (gram)
W_m	Saturated weight of ceramic sample
W_s	Suspended weight in the water (gram)
X	Distance between two layer
x	Distance to the contact surface, mm
α	Temperature coefficient of resistance (TCR) for the TPS element
$\bar{\alpha}$	Mean linear thermal expansion coefficient (K ⁻¹)
$\bar{\alpha}_A$	Mean linear thermal expansion coefficient correction for the apparatus over the temperature range
ρ	Bulk density (g/cm ³)
σ_{int}	Normal interface stress
σ_M	Maximum bending strength

LIST OF PUBLICATIONS

1. Uday M. Basheer, Ahmad Fauzi, M. N., Hasmaliza M., Ahmad Badri I., Effect of Rotational Speeds on the Friction Welding of Alumina- Aluminum 6061 alloy joints, *In proceedings of Malaysian Metallurgical Conference (MMC 2008)*. 2008: P. 22-25, UKM, Bangi, Malaysia.
2. Uday, M. B., Ahmad Fauzi, M. N., Zuhailawati H., Ismail A. B. Mechanical properties of Alumina-YSZ composite and 6061 Al Alloy joints fabricated by friction welding method, *In proceedings of Malaysian Metallurgical Conference '09 (MMC2009)*. 2009: P.1-5, Kuala Perlis, Perlis.
3. Uday M. B., Ahmad Fauzi, M. N., Zuhailawati H., Ismail A. B. Microstructural Observation of Friction Welded Alumina-Yttria Stabilized Zirconia (YSZ) Composite with 6061 Al Alloy, *RAMM & ASMP Conference 2009:P. 42-45*, Penang, Malaysia.
4. Ahmad Fauzi, M. N., Uday, M. B., Zuhailawati, H., Ismail, A. B., Microstructure and mechanical properties of alumina-6061 aluminum alloy joined by friction welding, *Materials & Design*, 2010, 31(2): p. 670-676.
5. Uday, M. B., Ahmad Fauzi, M. N., Zuhailawati, H., Ismail, AB, Advances in friction welding process: a review, *Science and Technology of Welding & Joining*, 2010, 15(7): p. 534-558.

6. Uday, M. B., Ahmad Fauzi, M. N., Zuhailawati H., Ismail A. B. Evaluation of interfacial bonding in dissimilar materials of YSZ-Alumina composites to 6061 aluminium alloy using friction welding, *Materials Science and Engineering: A*, 2011.528(25):p.1348-1359.
7. Uday M. B., Ahmad Fauzi M. N., Zuhailawati H., Ismail A. B. Effect of deformation behavior on the grain size of the 6061 aluminum alloy joint with alumina by friction welding, in *The International Conference on Experimental Mechanics and The 9th Asian Conference on Experimental Mechanics*, 2010:P. 97-102, Legend Hotel, Kuala Lumpur, Malaysia
8. Uday, M. B., Ahmad Fauzi M. N., Zuhailawati H., Ismail A. B. Effect of welding speed on mechanical strength of friction welded joint of YSZ-alumina composite and 6061 aluminum alloy, *Materials Science and Engineering: A*, 2011, 528(13-14): p. 4753-4760.
9. Uday M. B., Ahmad Fauzi M. N., Zuhailawati H., Ismail A. B. A study on the low rotational speed for the joining between YSZ-Alumina composite and 6061 Aluminum alloy by friction welding, *The 1st International conference on Materials Engineering and The 3rd AUN/SEED-Net Regional Conference on Materials*, Melia Purosani Hotel Yogyakarta, Indonesia, 2011: P. 51-55.

10. Uday, M. B., Ahmed Fauzi M. N., Zuhailawati H., Ismail A. B. Effect of Deformation Behavior on the Grain Size of the 6061 Aluminum Alloy Joint with Alumina by Friction Welding, *Applied Mechanics and Materials Journal*, 2011. 83: p. 97-103.
11. Uday M. B., Ahmad Fauzi M. N., Zuhailawati H., Ismail A. B. Thermal analysis of friction welding process in relation to the welding of YSZ-alumina composite and 6061 aluminum alloy, *Applied Surface Science Journal*, 2012, 258(20): p.8264-8272.

List of Exhibitions

1. Ahmad Fauzi Mohd Noor, Uday M. B., Zuhailawati H., Ismail A.B., “Ceramic-metal joining for advance thermal application”, *Malaysia Technology Expo (MTE 2010): Silver Medal*, 2010, 4-6 February 2010, Kuala Lumpur.
2. Ahmad Fauzi Mohd Noor, Uday M. B., Zuhailawati H., Ismail A.B., “MF welding of ceramic composites to 6061 Aluminum alloy”, *Malaysia Technology Expo (MTE 2011): Bronze Medal*, 2011, 21-24 February 2011, Kuala Lumpur Convention Centre (KLCC).

Kimpalan Geseran Aloi Aluminium 6061 dengan Komposit YSZ-Alumina untuk Tambahbaik Sifat Mekanik dan Terma

ABSTRAK

Dalam kajian ini, tiga jenis sistem utama digunakan bagi kimpalan geseran iaitu bagi cantuman aloi aluminium kepada alumina tulen, alumina dengan 25% berat YSZ, dan alumina dengan 50% berat YSZ. Sistem seramik difabrikasi dengan menggunakan kaedah penuangan slip dan disinter pada suhu 1600°C. Logam aloi aluminium pula dipotong dan digilap. Diameter rod seramik dan logam kedua-duanya berukuran 16 mm. Kesan parameter proses kimpalan geseran (kelajuan putaran, geometri sambungan dan tekanan yang digunakan) ke atas kimpalan bahan-bahan yang berlainan diteliti dan dikaji. Ujian terma bagi bahan dasar yang berlainan mempunyai peranan yang kuat ke atas pemanasan semasa geseran serta peningkatan suhu di antara dua permukaan. Hasil kajian ini menunjukkan bahawa alumina tulen boleh dicantum dengan aloi aluminium 6061 melalui kaedah kimpalan geseran pada kelajuan putaran 1250 dan 2500 rpm, manakala alumina dengan peratusan berat YSZ 25 dan 50% boleh dicantum pada kelajuan putaran yang lebih rendah (630 hingga 900 rpm). Kajian ini juga menunjukkan bahawa cantuman di antara alumina dengan 25% kandungan berat komposit YSZ dan aloi aluminium 6061 mempunyai kekuatan sambungan paling tinggi, kekerasan mikro yang rendah dan permukaan mikrostruktur yang baik pada kelajuan putaran 630 rpm berbanding sampel-sampel yang lain. Bagi sampel sambungan alumina tulen dengan aloi aluminium 6061, kekuatan sambungan melalui kimpalan geseran dipengaruhi oleh kelajuan putaran, di mana ia meningkat apabila kelajuan putaran meningkat. Kesan kelajuan putaran, geometri sambungan, masa kisan, tekanan kisan dan darjah

kecacatan permukaan lebih tinggi bagi aloi aluminium 6061 berbanding bahagian seramik. Peningkatan kelajuan putaran sewaktu kimpalan geseran mengakibatkan peningkatan kecerunan suhu dan pemendekan paksi, dimana lebih banyak jisim dikeluarkan daripada permukaan kimpalan. Kajian ini juga mendapati bahawa masa kisanan serta geometri permukaan seramik mempunyai kesan yang besar ke atas mikrostruktur sambungan, kekerasan mikro dan kekuatan lenturan. Data XRD menunjukkan bahawa perubahan dalam saiz hablur aloi logam, ketumpatan dan parameter kekisi berlaku pada kelajuan putaran yang berlainan. Saiz hablur didapati amat halus dan terhablur semula secara dinamik berdekatan dengan kawasan kimpalan. Walau bagaimanapun, saiz hablur ini mengalami pemanjangan apabila pelbagai jarak kawasan kimpalan. Parameter yang berlainan memberikan kesan keretakan samada mulur atau rapuh pada permukaan bahan.

Friction Welding of 6061 Aluminum Alloy with YSZ-Alumina Composite for Improved Mechanical and Thermal Properties

ABSTRACT

In the present work, three main dissimilar materials were used in friction welding i.e. 6061 aluminum alloy joined to pure alumina, alumina-25 wt. % YSZ and alumina-50 wt. % YSZ. The ceramic systems were fabricated by slip casting and subsequently sintered at 1600 °C, while the metal aluminum alloy was cut and polished. The diameter of both the ceramic and metal rods was 16 mm. The effects of friction welding process parameters (rotational speed, friction time, joint geometry and applied pressure) on the dissimilar material joints characteristics were evaluated. The thermal analysis of base materials plays an important role in the possibility of friction heat generation and increasing the friction temperature between two surfaces. The results in this study showed that pure alumina was able to be friction welded to 6061 aluminum alloy at rotational speeds between 1250 and 2500 rpm, while alumina-25, 50 wt. % YSZ were joined at lower rotational speeds (630 rpm to 900 rpm). It was also observed that joint between alumina – 25 wt % YSZ composite and 6061 aluminum alloy at lower rotational speed of 630 rpm produced the highest joint strength but lower microhardness with good microstructure as compared to the other ceramic components joint. On the other hand, the mechanical strength of friction-welded pure alumina / 6061 aluminum alloy components was affected by the rotational speed which increases in strength with increasing rotational speed. The effect of rotation speed, joint geometry, friction time, applied friction pressure and degree of deformation appears to be high on the 6061 aluminum alloy than on the ceramic part. The effect of increasing rotational speed over

the friction-welding joint was that both the temperature gradient and the axial shortening increased as a result of more mass being transferred out of the welding interface. The results also indicated that the friction time and ceramic face geometries have a significant effect on the joint microstructure, microhardness and bending strength. The XRD data showed that changes in metal alloy crystallite size, density and lattice parameters occurred over the test distances at different rotational speeds. The grains were fine and dynamically recrystallized near the weld interface and elongated after different distances. The fracture surfaces were different with different parameters giving either ductile or brittle failure.

CHAPTER 1

INTRODUCTION

1.1 Background

Ceramic-metal bonding is one of the biggest challenges that have faced manufacturers and users over the years because of the inherent differences in the thermal expansion coefficients of the two dissimilar materials. Nevertheless, several techniques have been developed to produce a good bonding, but it depends on the materials bonded. Among others, it includes solid state welding, direct diffusion bonding, hot isostatic pressing, reactive metal bonding and active metal brazing (Nascimento et al., 2003; Noh, 2008). There were several factors influencing the degree of success when joining of different materials are attempted; these include the properties of the interface created in the joint and the thermal expansion coefficient mismatch between the joined materials, which potentially results in forming of large residual stresses during cooling of the joined materials. In order to overcome these problems, friction welding could be the technique for producing high integrity joints. Friction welding is reported to be one of the most economical and highly productive methods in joining similar and dissimilar metals, although it is relatively unknown in joining of metal to ceramics. It is widely used in automotive, aerospace industry and engineering applications (Sathiya et al., 2007).

Friction welding is a solid state joining that produces a bond under the compressive force of one rotating workpiece to another stationary workpiece

(Akbarimousavi and Goharikia, 2011). Heat is generated at the weld interface during friction welding because of the continuous rubbing of contact surfaces, which, subsequently results in softening of the metal. Eventually, the material at the interface starts to flow plastically and forms an upset (Mousavi and Kelishami, 2008). When certain amount of forging had occurred, the rotation stops and the compressive force is maintained or slightly increased to consolidate the weld. Some of the important operational parameters in friction welding are friction time, friction pressure and rotation speed (Özdemir et al., 2007).

For a particular application, heating time is determined during the set-up or from previous experience. Excessive heating limits productivity and increase wastes material. Similarly, uneven heating as well as entrapped oxides causing unbonded areas at the interface may be due to insufficient welding time. The effective pressure ranges are also broad for heating and forging although the selected pressure should be reproducible for any specific operation. The pressure controls the temperature gradient in the weld zone, the required drive power and the axial shortening (Khan, 2012). The specific pressure depends upon the materials being joined and the joint geometry.

On the other hand, the rotational speeds are related to the material to be welded and the diameter of the weld at the interface. They might have different effects upon the mechanical properties of friction joints. Increasing rotational speed might lead to greater frictional heat at the interface, consequently leading to softening of the metal, a greater extent of recrystallization, or even increased intermetallic formation (Yeoh et al., 2004). Additionally, depending upon the type of materials joined or more accurately, the

mechanical and physical properties involved, different ranges of rotational speeds would produce different effects on the quality of the joint. Therefore, appropriate rotational speeds must be used to minimize any detrimental effects and produce joints of good quality.

Many researchers have carried out different studies on the interface microstructure and mechanical properties of the friction welding. For example, Özdemir (2005) had joined AISI304L austenitic stainless steel and AISI4340 steel by friction welding using different rotational speeds in their studies. He found that the tensile strength of the joints was markedly affected by the joining rotational speed chosen. They have also studied the effect of rotational speed on the interface properties of friction welded of different kind of steel (Özdemir et al., 2007). They observed that the width of the full plastic deformed zone (FPDZ) has an important effect on the strength of friction welded samples and the strength increases with increase of the rotational speed. (Noh et al., 2008) had joined Al_2O_3 with mild steel by friction welding using Al sheet as an interlayer. The strength of Al–steel bonding was dependent on the wettability of the alumina surface by the partially molten Al interlayer with constant rotational speed.

Work by Avinash et al. (2007) showed the feasibility of producing similar metal joints of titanium alloy by rotary friction welding method by using three different rotational speeds. They observed that in all the three cases of rotational speeds, the weld joints were continuous and the Heat Affected Zone (HAZ) was very thin. However, there was a distinction between the microstructures developed near the interface in the two joints, such as the grains had enlarged or reduced in size. In others, Lin et al. (1999)

studied the effect of joint design and volume fraction on friction welding properties of Al / SiC composites. They found that the HAZ consisted of three zones, i.e. fully plasticized region, partially deformed region and the undeformed region. Mortensen et al. (2001) conducted bending tests on welded and non-welded 416 stainless steel. In all samples, the bending strength decreased with decrease in the ductility of the welding samples.

1.2 Problem Statement

Friction is a very important aspect in friction welding since the process itself relies on the heat generated from the frictional force between rotary workpiece to stationary one to soften and subsequently the joining. Although this welding technique has been successfully developed and applied in various cases in industries, the friction phenomena during ceramic to metal joining is not yet fully understood. Therefore, this study addresses the friction welding process between the ceramic and the metal interface, between the surfaces microstructure interface as well as the mechanical and thermal properties in the joining.

The majority of the techniques used today are based on the joining of ceramics with metals either by diffusion bonding, active metal brazing, brazing with oxides and oxynitrides, or diffusion welding (Martínez Fernández et al., 2000; Cook and Sorensen, 2011). These techniques need either very high temperatures for processing or hot pressing (high pressures). The joints produced by these techniques have different thermal expansion coefficients than the ceramic materials, which creates a stress concentration in the joint area (Lemus-Ruiz et al., 2008). The high stress sometimes

results in joint failures or unreliable joints. Therefore, the thermal stress problems should be overcome to obtain reliable joints between the ceramic and the metal. The ceramic and metallic components should be selected with minimal thermal expansion differences throughout their operating range. In addition to the previously mentioned problems, the active metal brazing requires a stringent firing atmosphere, either high vacuum or reducing gas conditions to prevent the active species (Darsell and Weil, 2007). This represents a high capital expense and higher operating cost.

In order to overcome those problems mentioned above, the friction welding could be an interesting and cost effective alternative, provided that the strength of friction welded joints reaches or exceeds the strength of those joints produced by other techniques (Weiss and Sassani, 1998; Noh et al., 2008).

The friction welding of dissimilar materials is more complicated than similar materials due to difference in the physical, thermal, chemical and mechanical properties of base materials (Khan, 2011). The weld strength and its interface properties are extremely important. The failure of these welded parts may lead to huge losses. Therefore, the quality of weld is extremely important. In friction welding of dissimilar materials combinations such as 6061 Al alloy - Stainless steel 304, 5052 Al alloy – stainless steel 304, the weld strength and its interface properties are degraded due to formation of intermetallic compounds. These compounds strongly depend on the local temperature attained during the welding process and they are responsible for brittle failure of the components. However, there is possibly non-uniform heat generation

across the weld interface as the rotational speed of inner region is less than outer region, and thus heat generated in the inner region is less than outer region.

To overcome the above problems the progression of friction welding process is important to be investigated. In regular friction welding process the development of friction weld starts from the outer periphery and it progresses to inner region which increases the severity of above problems (Khan, 2011). The welding process is improved by reversing the progression of welding and this is achieved by designing a new joint geometry. The new joint geometry (taper pin 30°, taper pin 60° and pin) reverses the progress of friction welding from inner region to outer periphery. The comparison and detail explanation of the proposed new joint geometry and its influence are discussed in detail in subsequent sections, which shall be part of the research emphasis.

The new methods of friction welding are becoming more widely implemented in the manufacture of aero engines, because these solid phase joining processes provide high weld quality and economic benefits (Kallee et al., 2003). High-strength metal alloys are of interest for structures requiring minimum weight, especially in the aerospace industry. Along with the interest in high-strength metal alloys, there is a growing requirement to join ceramic composite components. For high-performance applications an improved strength / toughness combination is needed, and for this reason the solid phase friction welding processes have been developed, as they are likely to have a good balance of properties in the materials. Friction welding processes also permit the joining of dissimilar materials, thus making best use of specific material properties at the operating location.

Therefore, the joining of 6061 Al alloy and Al₂O₃-YSZ composites explained in this study. The 6061 Al alloy was selected for this study because of the cheaper cost as compared to other Al alloys. This alloy is widely used in aerospace and automobile industries. Meanwhile, the Al₂O₃-YSZ ceramic composite samples were prepared using most cost effective slip casting technique. YSZ reported to be ceramic material having good toughness properties (Cesari et al., 2006) than pure Al₂O₃, therefore making a composite with Al₂O₃ leads to a more durable ceramic material for many applications. The other reason for these selected materials was to produce a novel metal alloy-ceramic composite joining by friction welding technique, which also provides a new data analysis system for future researchers.

1.3 Objectives of the Research

The primary objectives of this research are as follows:

1. To study the parameters in friction welding that would be able to produce good mechanical bending strength i.e. friction time, rotational speeds and friction pressure with constant forging pressure and time on the joining between two dissimilar materials.
2. To study the effect of different specimen geometry faces on the strength of the friction welded joint with 6061 Al alloy.
3. To assess the correlation between thermal properties of base materials, friction temperature and heat generation with interfacial microstructural behavior.
4. To characterize the evolution of microstructure in the 6061 Al alloy deformation regions and relate it to the friction welding parameters.

1.4 Research Approach

This research was divided into three stages; Al_2O_3 -YSZ composite preparation, 6061 Al alloy preparation and thirdly is the joining process. In the first stage, the Al_2O_3 -YSZ composite rods were prepared through slip casting and in the second stage the Al metal alloy rods were machined into required diameters. Figures (1.1, 1.2 and 1.3) show the flowchart of the various stages in this research. The effect of the various parameters investigated (rotational speed, friction time, joint geometry and friction pressure) were characterized for their physical and mechanical properties, as well as plastic deformation and the microstructure developed after friction welding.

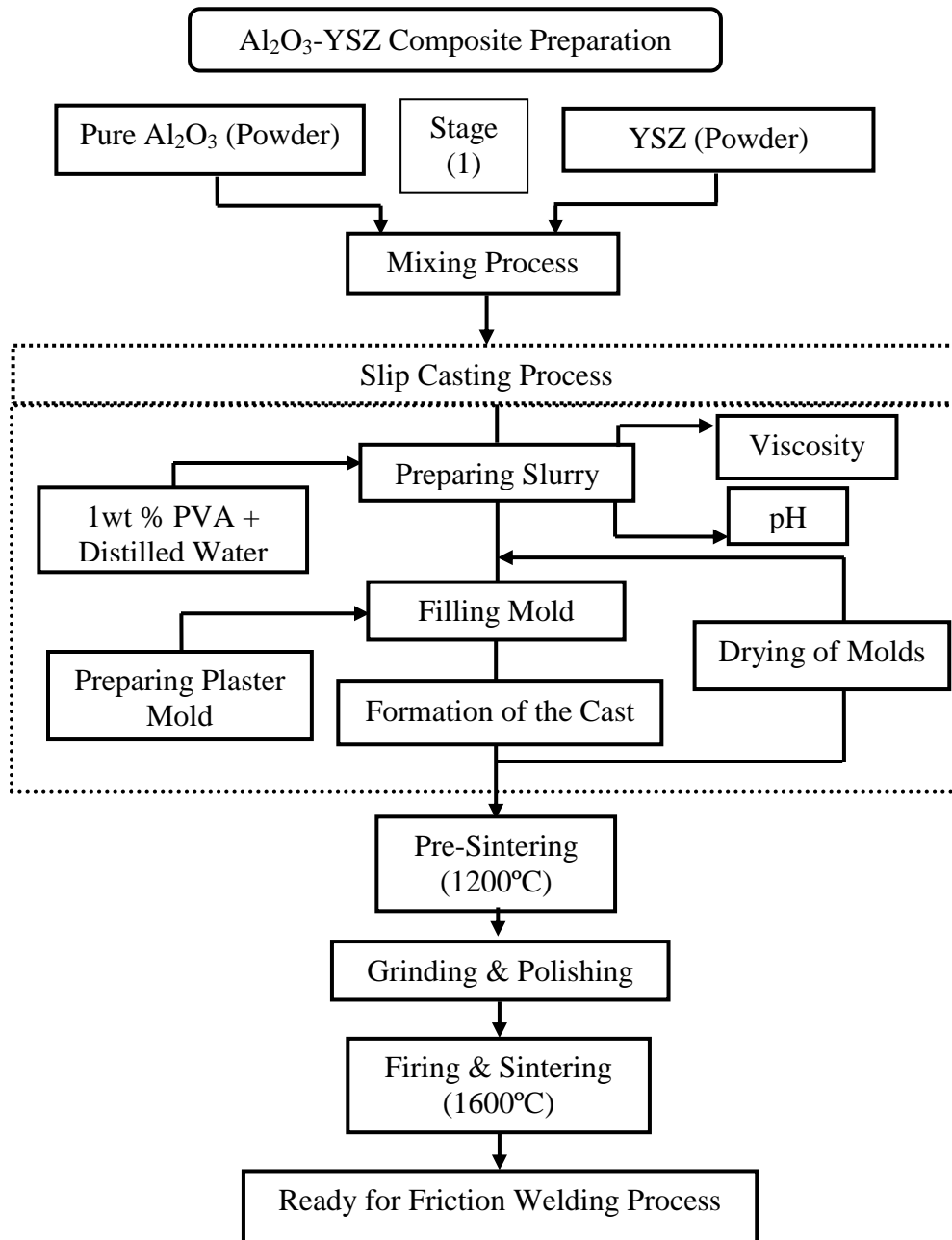


Figure 1.1: Flowchart of research stage one, ceramic composite preparation

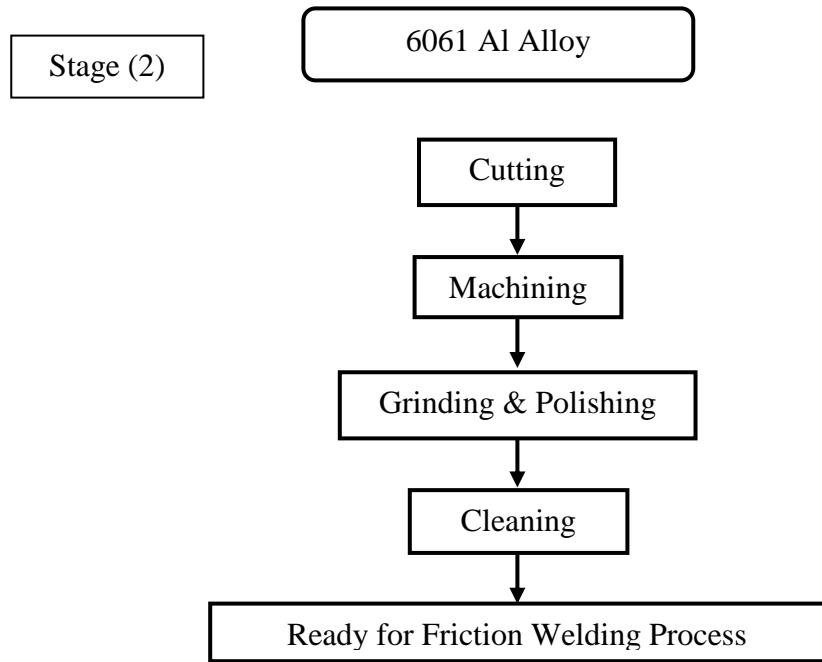


Figure 1.2: Flowchart of research stage two, 6061 Al alloy preparation

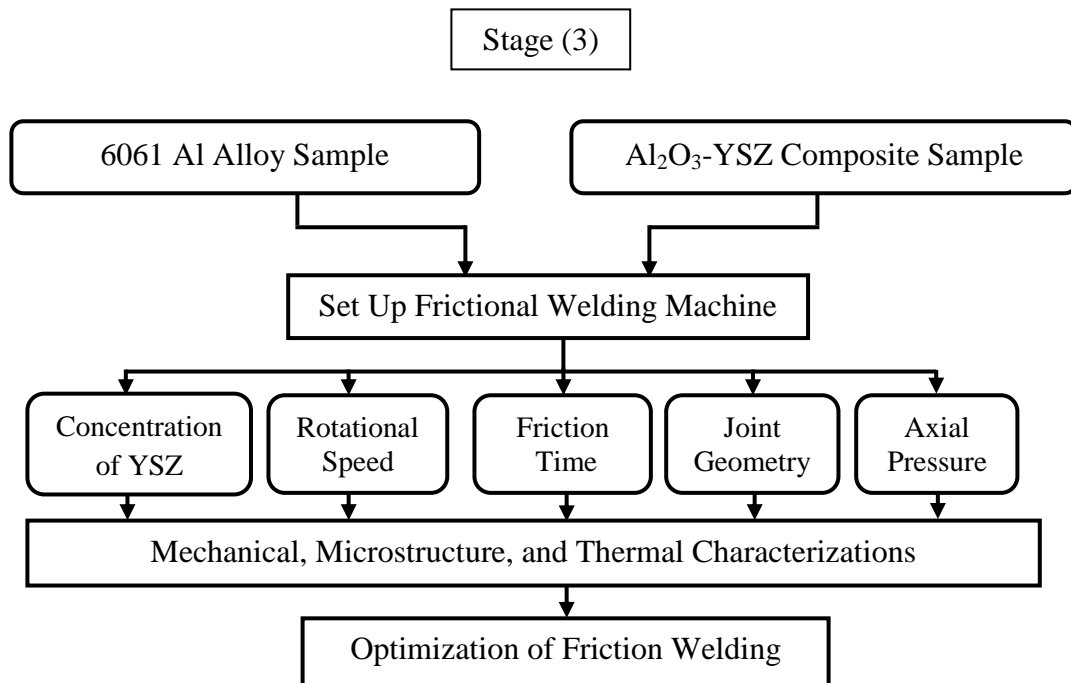


Figure 1.3: Flowchart of research stage three, friction welding process

CHAPTER 2

LITERATURE REVIEW

2.1 Friction Welding

Friction welding (FW) is a solid state joining method (meaning the metal is not melted during the process) which produces coalescence of materials under compressive force when the workpieces rotate or move relative to each other (Woo et al., 2002; Skrotzki, 2008) producing heat and plastically displacing the material from the faying interface. While considering a solid-state welding process, under some circumstances a molten film may be produced at the interface. However, even then the final weld should not exhibit evidence of a molten state because of extensive hot working during the final stage of the process. Filler metal, flux, and shielding gas are not required in this process (O'Brien, 1991; Nguyen and Weckman, 2006; Maalekian, 2007). The basic steps involved in friction welding are shown in Figure 2.1.

Initially, one workpiece is rotated while the other is kept stationary as shown in Figure 2.1(a). When the appropriate rotational speed is reached, the two workpieces are brought together and axial force is applied as shown in Figure 2.1 (b). Rubbing at the interface heats the workpiece locally and upsetting starts, as shown in Figure 2.1(c). Finally, rotation of one of the workpieces is stopped which completes the upsetting (Figure 2.1d). The friction weld produced is characterized by a narrow heat affected zone, the presence of plastically deformed material around the weld (flash), and the absence of a fusion zone.

Friction welding as a method of joining was first patented in the 1890's by an American named Bevington (Nicholas, 2003). References are also known which indicate that the 'spin welding' of plastics was carried out in the 1930s to 1940s. However, its impact on welding metals wasn't so prominent until 1956s when the process was advanced significantly by Soviet workers (Lee et al., 2003). Further time elapsed before the process was introduced into the UK and USA in the early 1960's.

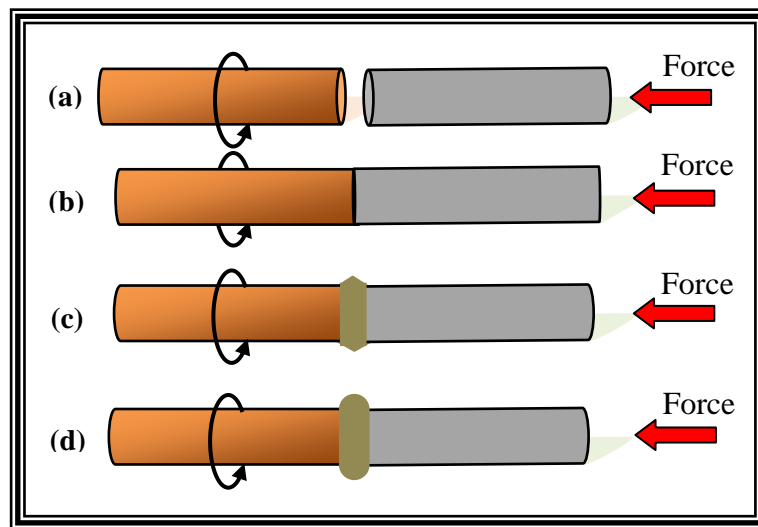


Figure 2.1: Basic steps in friction welding (Maalekian, 2007; Kalsi and Sharma, 2011)

2.1.1 Energy Input Methods in Friction Welding

There are two methods of supplying energy in friction welding. Direct drive friction welding, sometimes called conventional friction welding and uses a continuous input. Inertia friction welding, sometimes called flywheel friction welding uses energy stored in a flywheel.

2.1.1.1 Direct Drive Welding

Direct-drive friction welding is a well-established solid-state joining process (Davis, 2000) which can be used to join a wide range of conventional steel alloys as well as more metallurgically challenging systems such as dissimilar metal combinations and super alloys (Fortulan and Souza, 1999). In this process (Figure 2.2), one of the workpieces is attached to a motor driven unit while the other is restrained from rotation (Nicholas, 2003). The motor driven workpiece is rotated at a predetermined constant speed. The workpieces to be welded are moved together and then a friction welding force is applied. Heat is generated as the faying surfaces (weld interface) rub together. This continues for a predetermined time or until a preset amount of upset takes place. The rotational driving force is discontinued and the rotating workpiece is stopped either by the application of a braking force or by its own resistance to rotation. The relationship of direct drive friction welding parameter characteristics is shown in Figure 2.3.

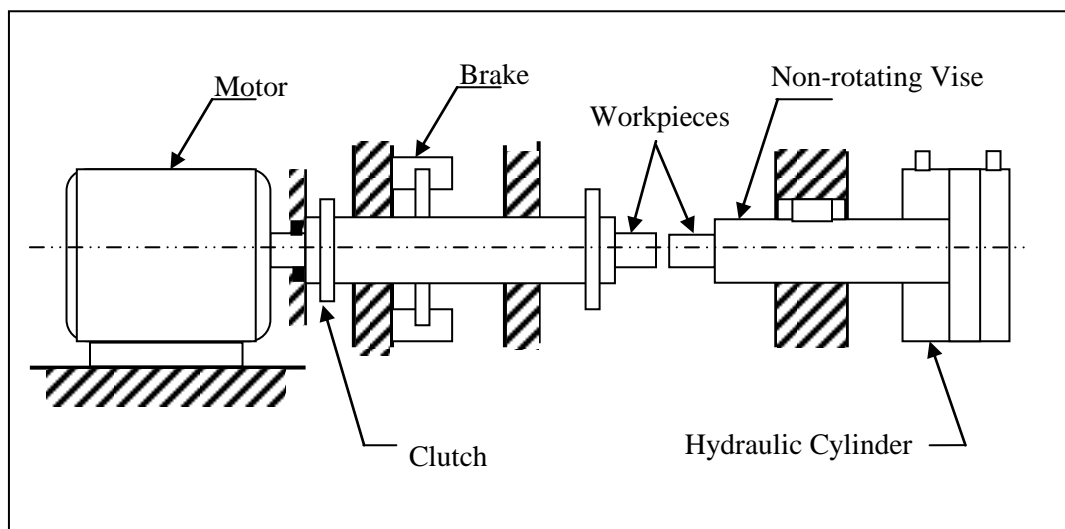


Figure 2.2: Basic arrangement of a direct drive-welding machine (Sahin, 2009c)

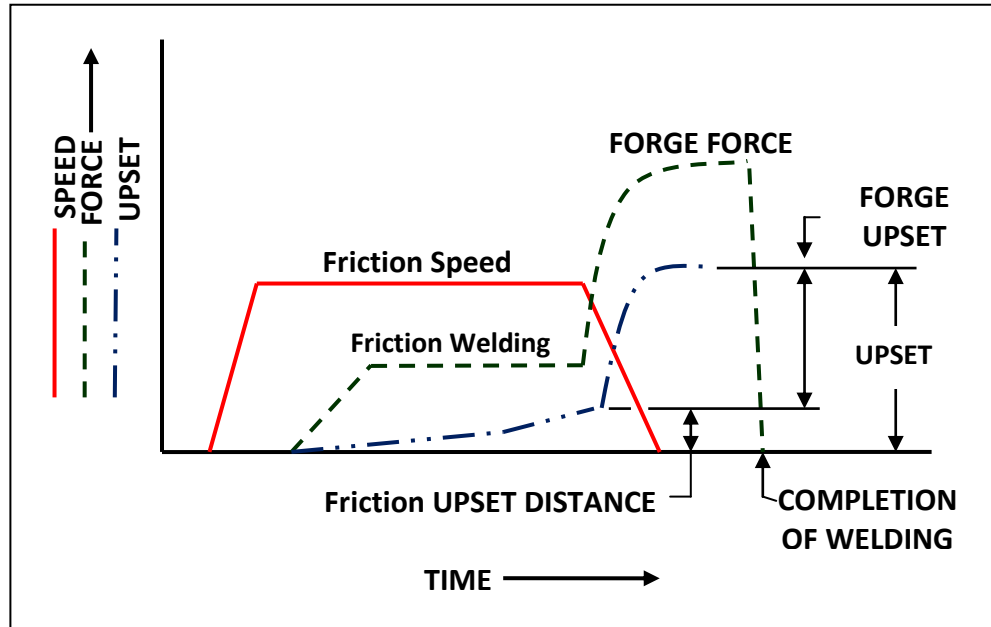


Figure 2.3: Direct drive friction welding parameter characteristics (Maalekian, 2007)

2.1.1.2 Inertia Drive Welding

Inertia drive welding is the most popular method for the joining of axisymmetrical parts in which one workpiece is rotated as the two workpieces are brought together under friction pressure (Li et al., 2007). In inertia friction welding (Figure 2.4), according to some researchers, one of the workpieces is connected to flywheel while the other is restrained from rotating (O'Brien, 1991; Mortensen et al., 2001; Daus et al., 2007). The flywheel is accelerated to a predetermined rotational speed to store the required energy. The drive motor is disengaged and the workpieces are forced together by a friction welding force. This causes the faying surfaces to rub together under pressure. The kinetic energy stored in the rotating flywheel is dissipated as heat through friction at the weld interface thus welding the two surfaces together as the flywheel speed decreases. An increase in friction welding force may be applied (forge force) before rotation stops (Nicholas, 2003; Sahin, 2007; Sahin, 2009a; Sahin,

2009c). The forge force is maintained for a predetermined time after rotation ceases. The relationship of inertia friction welding parameter characteristics appears in Figure 2.5.

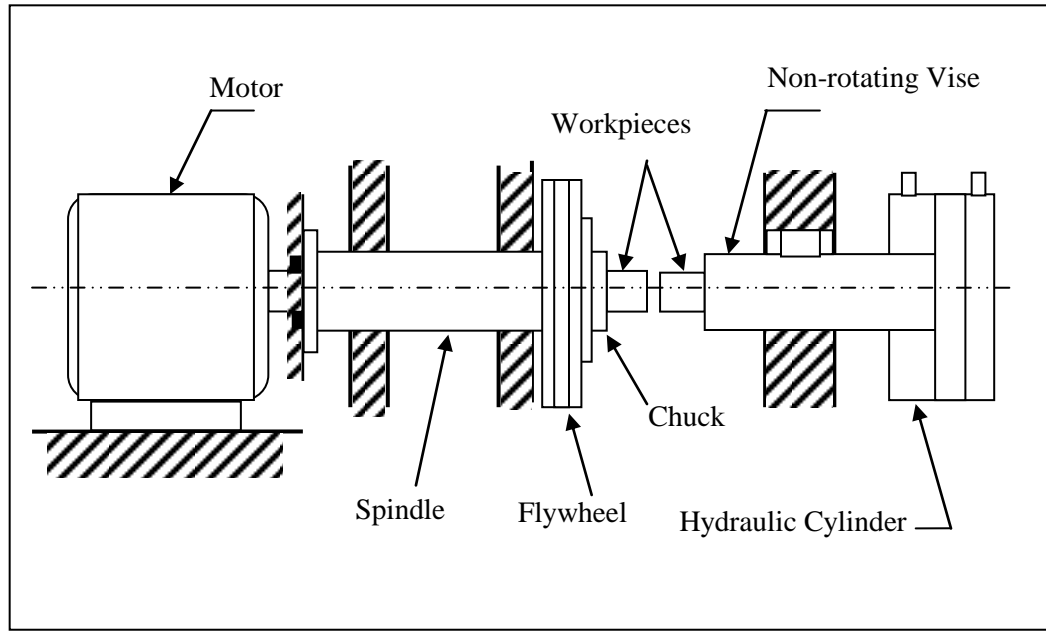


Figure 2.4: Basic arrangement of an inertia-welding machine (Izadi, 2008)

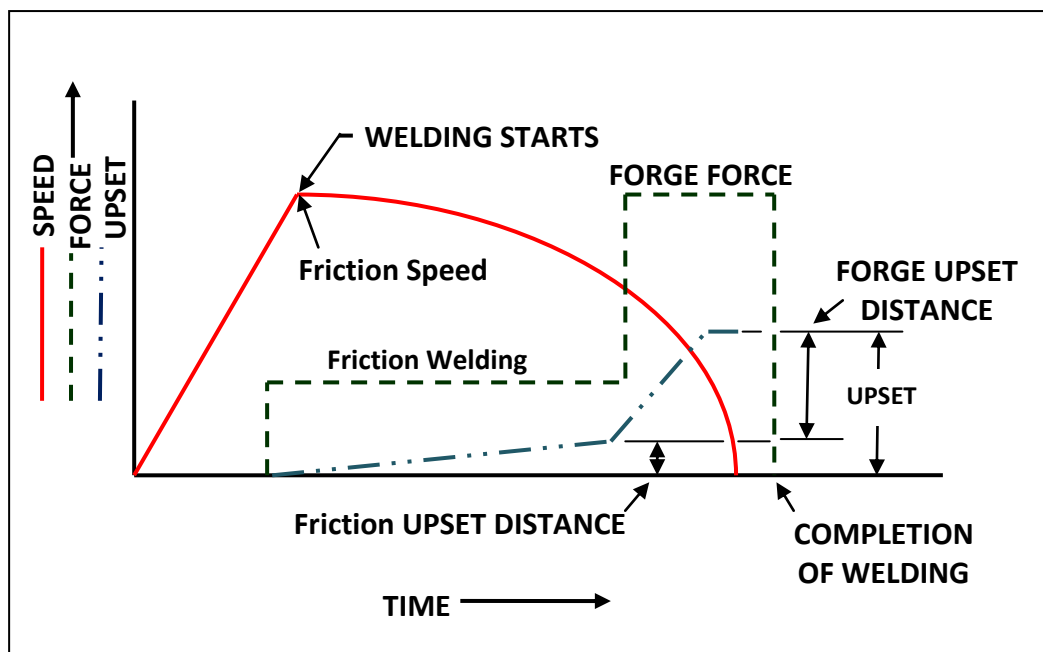


Figure 2.5: Inertia friction welding parameter characteristics (Maalekian, 2007)

2.1.2 Types of Friction Welding

Welding is a widespread and versatile technique for joining two pieces of the same or different kind of material. A lot of different types of welding are used; one of them is friction welding. Friction welding involves forcing two pieces of metals together with sufficient force to bond together. Advantages of friction welding over other welding types include its relatively low power requirements, simplicity of the operation and the rapid dissipation of the heat generated by the friction.

2.1.2.1 Rotary Friction Welding

Rotary friction welding is one of the solid-state techniques that is applied to join similar or dissimilar materials (Kurt et al., 2011). The rotary friction welding process is inherently flexible, robust and tolerant to different qualities of materials. The parameters involved are the rotational speed, time and force applied. However, as the process is inherently robust and flexible, deviations on these parameters can still give a good weld. It is widely used by various industries (Nicholas, 2003; Davari et al., 2011).

In this technique, machinery components are brought into contact. While one of them remains stationary, the other is rotated with the applied pressure (Figure 2.6). When the temperature of the interfaces has reached to an optimum value for the extensive plastic deformation, the rotation is stopped, while the forging pressure remains unchanged or increased. The application of an axial force maintains intimate contact between the parts and causes plastic deformation of the material near the weld interface of the weld. The rotating speed and applied pressure affect the shape of welded zone and the width of HAZ. Application of high pressure produces narrow HAZ, while using high

rotating velocity causes extension of HAZ and enlarged grain sizes (Davari et al., 2011). Also HAZ width changes with thermal conductivity variation of the used material. Ordinarily, if the variations of parameters lead to increase of mechanical energy, HAZ will be extended.

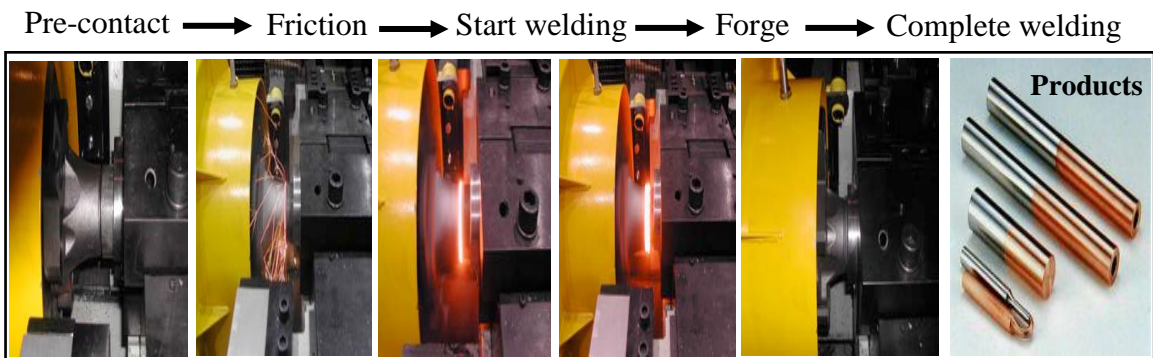


Figure 2.6: Rotary friction welding process (Sanders, 2001)

2.1.2.2 Orbital Friction Welding

Orbital friction welding is a type of friction welding (Figure 2.7) which is particularly suited for the joining of non-circular cross-section components (Maalekian, 2007). This type of friction welding is similar to rotary friction welding but both welded parts are rotated in the same direction at the same speed. In this application, neither workpiece rotates around its central axis. The orbital motion provides uniform tangential velocity over the total interface area. When motion ceases, the parts are realigned quickly. Practically it has been recognized that the high quality welds are produced using this process which is attributed to the constancy of the relative velocity at the rubbing interface. Also this process has important advantages such as a uniform rate of heat generation at the rubbing interface that produces a uniform thickness of the heat affected zone (HAZ) and the cross-section of the components can be of any shape.

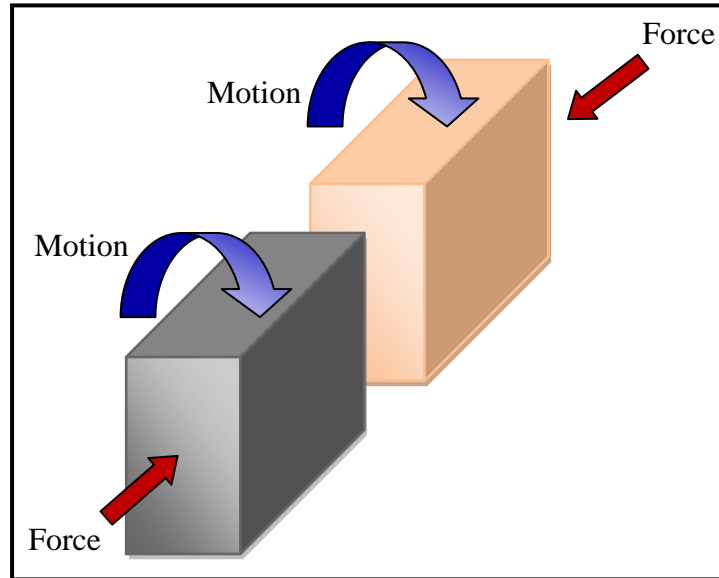


Figure 2.7: Schematic diagram of the orbital friction welding process (Davim et al., 2008)

2.1.2.3 Linear Friction Welding

Linear friction welding (LFW) is a solid state joining process in which a stationary part is forced against a part that is reciprocating in a linear manner to generate frictional heat (Bhamji et al., 2011). The heat, along with the force applied perpendicular to the weld interface, causes material at the interface to deform and plasticize (Figure 2.8). Much of this plasticized material is removed from the weld, as flash, because of the combined action of the applied force and movement of the part. Surface oxides and other impurities are removed, along with the plasticized material, and this allows metal to metal contact between parts and allows a joint to form (Jun et al., 2010; Bhamji et al., 2012).

This process offers advantages over fusion welding when joining metals that exhibit solidification problems (e.g. porosity, hot cracking, segregation, etc.). In addition, in most cases the severe deformation in the weld region during friction welding

results in a refined microstructure, which can provide improved strength at the weld line relative to the parent material. On the other hand, the main disadvantage of this process is the high capital cost of the equipment. The high cost of both the equipment and tooling means the LFW process can only be justifiably used for producing high value added components (Wanjara and Jahazi, 2005). This has generally confined the process to niche applications such as producing bladed discs for aero engines. However, machines based on the principle of stored energy, rather than direct drive, have significantly lowered costs and this may mean the LFW of lower value added components can be justified. A further disadvantage of the process is that it can be very noisy.

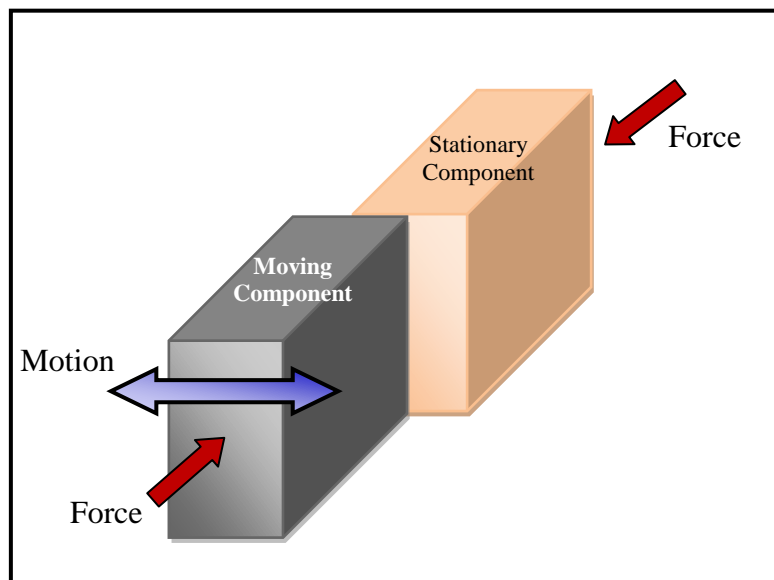


Figure 2.8: Schematic diagram of the linear friction welding process (Jun et al., 2010)

2.1.2.4 Radial Friction Welding

At the effect of radial pressure, the friction heat generated in friction interface is used to heat the welding zone to a high temperature, and then a large radial forging force

is applied to the radial friction welding process, which is particularly suitable for welding rotator structures, such as tubular and annular workpieces (Luo et al., 2012). This process can be used to join circular sections where it is undesirable to rotate the parts to be joined. It is also used to weld collars to shafts and tubes. As shown in Figure 2.9, the applied force on the rotating band is perpendicular to the axis of rotation. The collar is rotated and compressed as it is heated. An internal expanding mandrel supports the pipe walls and prevents penetration of upset metal into the bore of the pipe.

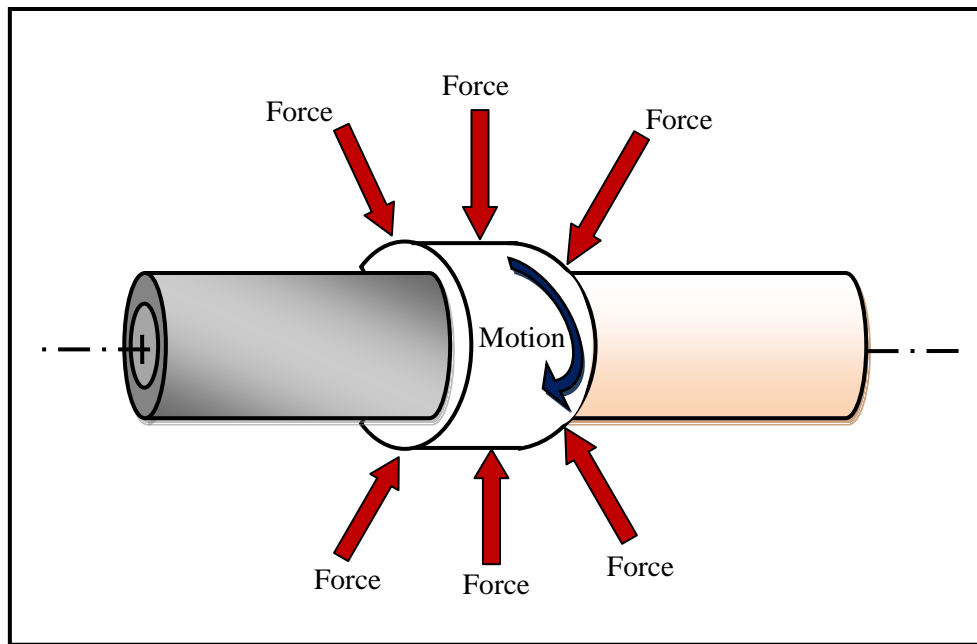


Figure 2.9: Schematic diagram of the radial friction welding process (Luo et al., 2012)

2.1.2.5 Friction Stir Welding

Friction-stir welding (FSW) is a solid-state joining process and is used for applications where the original metal characteristics must remain unchanged as far as possible (Harris and Norman, 2003; Schwartz, 2011; Huang et al., 2012). This process is

primarily used on Al, and most often on large pieces which cannot be easily heat treated post weld to recover temper characteristics. In this technique, a non-consumable tool is rotated and traverses through the material to be joined forming a plasticized annulus around the central pin whereby material is transferred from the front to the back of the pin, eliminating the joint interface (Figure 2.10) (Threadgill, 2007). More recently, FSW has been increasingly employed for aluminium alloys in the ship building and aerospace industries. The first fully friction stir welding component, a cylindrical intermediate assembly, was launched from Cape Canaveral in 1999. In parallel with the many current industrial applications with aluminium, friction stir welding is also being developed for joining copper, titanium and steels.

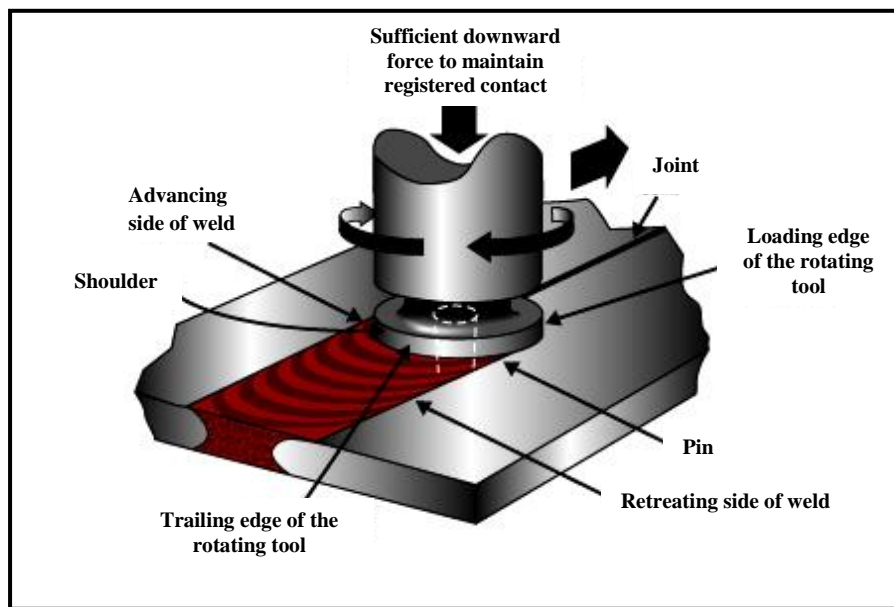


Figure 2.10: Friction stir welding process (Liechty, 2007)

2.1.3 Types of Relative Motion in Friction Welding Process

With most friction welding applications, one of the two workpieces is rotated about an axis of symmetry with the faying surfaces perpendicular to that axis. This means that in the normal case, one of the two workpieces must be circular or tubular in

cross section at the joint location (Robert, 1999). Typical arrangements for single and multiple welding operations are shown in Figure 2.11 (A) through (E).

Figure 2.11 (A) depicts the conventional and most commonly used in which one workpiece rotates while the other remains stationary. Figure 2.11 (B) shows another mode in which both workpieces are rotated, but in opposite directions. This procedure would be suitable for producing welds where very high relative speeds are needed. Figure 2.11 (C) shows a third mode where two stationary workpieces push against a rotating piece positioned between them. This setup might be desirable if the two end parts are long or are of such an awkward shape that rotation would be difficult or impossible by the other modes.

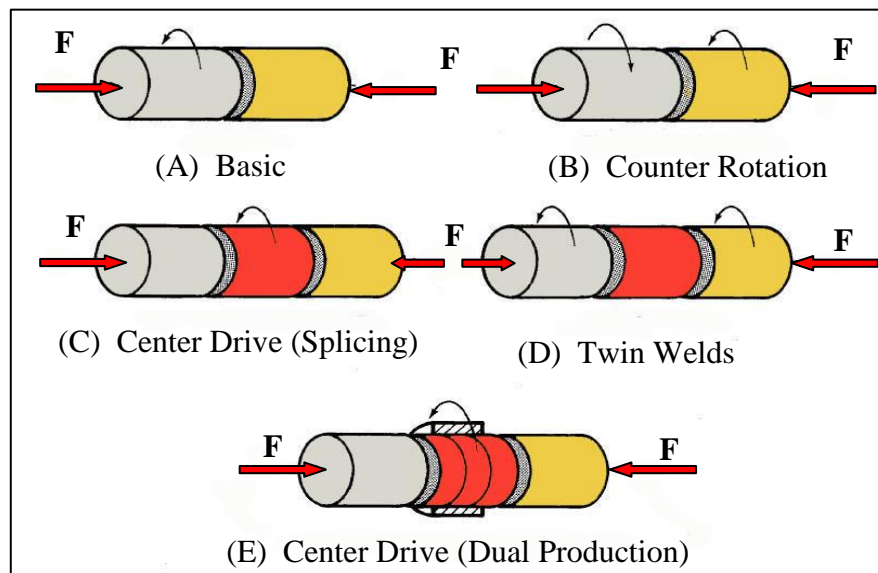


Figure 2.11: Typical Arrangements of Friction Welding (Robert, 1999)

A similar situation, shown in Figure 2.11 (D) involves two rotating pieces pushing against a stationary piece at the middle. The same principle can be applied to

the making of two welds back to back at the same time with one rotating spindle at the center, as shown in Figure 2.11 (E), for the purpose of improving productivity.

2.1.4 Advantages and Limitations of Friction Welding Process

Friction welding, like any welding process, has its specific advantages and disadvantages. The following are some advantages of friction welding such as no filler metal is needed. Flux and shielding gas are not required. The process is environmentally clean, no arcs, sparks, smoke or fumes are generated by clean parts (Kumar et al., 2010). Surface cleanliness is not as significant, compared with other welding processes, since friction welding tends to disrupt and displace surface films. There are narrow heat affected zones. The process is suitable for welding most engineering materials and is well suited for joining many dissimilar material combinations. In some cases, the weld strength is stronger than the weaker of the two materials being joined. Operators are not required to have manual welding skills. The process is easily automated for mass production. Welds are made rapidly compared to other welding processes. Plant requirements (space, power, special foundations, etc.) are minimal.

There are also some limitations of the process like; one workpiece must have an axis of symmetry and be capable of being rotated about that axis. Preparation and alignment of the workpieces may be critical for developing uniform rubbing and heating, particularly with diameters greater than 50 mm. Capital equipment and tooling costs are high. Dry bearing and non forgeable materials cannot be welded. If both parts are longer than 1 m, special machines are required. Free- machining alloys are difficult to weld.

2.1.5 Mechanism of Friction Welding

While specific details of the bonding process are unclear, the welding cycle can be divided into two stages; the rubbing or friction stage and the upsetting or forging stage. The welding heat is developed during the first stage and the weld is consolidated and cooled during the second stage.

2.1.5.1 Friction Stage

When the pieces make contact, rubbing takes place between the faying surfaces while the strong adhesion takes place at various points of contact. The unit pressure is high. At some points, the adhesion is stronger than the metal on either side. During the process, shearing takes place and the metal is transferred from one surface to the other. As rubbing continues, both torque and the interfacial temperature increase. The sizes of the transferred fragments grow until they become a continuous layer of plasticized metal. If a liquid film forms, it occurs at this point. During this period, the torque peaks and decreases to some minimum value which remains reasonably constant as metal is heated and forced from the interface while axial shortening continues (O'Brien, 1991; Kimura et al., 2003).

2.1.5.2 Forging Stage

Toward the end of the heating process, forging pressure is applied to the workpiece to cause axial shortening. This upset results in the flash as shown in Figure 2.1(d). Comparing Figure 2.3 with Figure 2.5, it can be seen that the latter part of the direct drive and inertia friction welding processes are very similar with respect to axial shortening (upset), speed and pressure. As the speed decreases, a second torque peak